Structural Engineering and Mechanics, *Vol. 61, No. 4 (2017) 441-451*
DOI: https://doi.org/10.12989/sem.2017.61.4.441

RBDO analysis of the aircraft wing based aerodynamic behavior

Rabii El Maani[*1,2], Abderahman Makhloufi[1a], Bouchaïb Radi[2b] and Abdelkhalak El Hami[1c]

[1]*LOFIMS, INSA de Rouen, Avenue de l'Université, 76800 Saint Etienne de Rouvray, France*
[2]*LIMII, FST Settat, route de Casablanca, Settat, Morocco*

(Received May 4, 2016, Revised October 1, 2016, Accepted October 21, 2016)

Abstract. The need of progress in engineering designs especially for aerospace structure is nowadays becoming a major industry request. The objectives of this work are to quantify the influence of material and operational uncertainties on the performance of the aerodynamic behavior of an Aircraft Wing, and to give a description of the most commonly used methods for reliability based design optimization (RBDO) to point out the advantages of the application of this method in the design process. A new method is proposed, called Safest Point (SP) that can efficiently give the reliability-based optimum solution for freely vibrating structures with and without fluid flow.

Keywords: fluid-structure interaction; aircraft wing; aerodynamic; reliability; RBDO; uncertainties

1. Introduction

Fluid-structure interaction (FSI) is a multiphysics phenomenon that occurs in a system where flow of a fluid causes a solid structure to deform which, in turn, changes the boundary condition of a fluid system. This can also happen the other way around where the structure makes the fluid flow properties to change. This kind of interaction occurs in many natural phenomena and man-made engineering systems. It becomes a crucial consideration in the design and analysis of various engineering systems. For instance, FSI simulations are conducted to avoid flutter on aircraft and turbomachines (Yun and Hui 2011), to evaluate the environmental loads and dynamic response of offshore structures and in many biomedical applications.

Using a validated 3D FSI model which consists on a steady aerodynamic analysis and static aeroelastic simulations of transonic wing. The fluid and the structure were modeled independently and exchanged boundary information to obtain aeroelastic solutions. The fluid was modeled using a computational fluid dynamics solver based on finite volume method (Fluent) and the structure was modeled using finite element approximation (ANSYS/Mechanical) and the two disciplines were loosely coupled in one-way direction.

In the Reliability Based Design Optimization (RBDO) model, the mean values of uncertain system variables are usually applied as design variables, and the cost is optimized subject to prescribed probabilistic constraints as defined by a nonlinear mathematical programming problem (Abbasnia *et al.* 2014). Therefore, an RBDO solution that reduces the structural weight in uncritical regions does not only provide an improved design but also a higher level of confidence in the design. The classical RBDO approach allows us to satisfy a required reliability level, but the vector of variables here contains both deterministic and random variables, which leads to a more complex problem than that of deterministic design. The major difficulty lies in the evaluation of the structural reliability, which is carried out by a special optimization procedure. So there is a strong motivation to develop a new technique that can overcome both drawbacks.

In this paper, we propose a new method, called Safest Point (SP) method that can efficiently give the reliability-based optimum solution relative to the Hybrid Method (HM) in order to solve the freely vibrating structures for the design undergoing fluid-structure interaction phenomena, and the applicability of the proposed framework to realistic design problems.

2. Fluid-structure interaction problem

A general fluid-structure interaction problem consists of the description of the fluid (Ω_f) and solid (Ω_s) domains, appropriate fluid-structure interface conditions at the conjoined interface and conditions for the remaining boundaries, respectively.

In the following, the fields and interface conditions are introduced; furthermore, a brief sketch of the solution procedure for each of the fields is presented.

2.1 About the fluid

All kinds of fluid flow and transport phenomena are

∗Corresponding author, Ph.D.
E-mail: rabii.el_maani@insa-rouen.fr
[a]Ph.D.
E-mail: abderahman.makhloufi@insa-rouen.fr
[b]Professor
E-mail: bouchaib.radi@yahoo.fr
[c]Professor
E-mail: abdelkhalak.elhami@insa-rouen.fr

http://www.techno-press.org/?journal=sem&subpage=8 ISSN: 1225-4568 (Print), 1598-6217 (Online)

governed by basic conservation principles such as conservation of mass, momentum and energy. All these conservation principles are solved according to the fluid model, which gives a set of partial differential equations, called the governing equations of the fluid. The following part elaborates on the theoretical background of Computational Fluid Dynamics (CFD) and the way it is employed for this particular case (Versteeg and Malalasekera 2007).

The continuity equation for a compressible fluid can be written as follows:

$$\frac{\partial \rho}{\partial t} + div(\rho \mathbf{v}) = 0 \tag{1}$$

Where ρ represents the density and $\mathbf{v}$ represents velocity of the fluid. The first term of the equation is the rate of change of density with respect to time and the next term is net flow of mass out of the element boundaries.

Newton's second law states that the rate of change of momentum of a fluid particle equals to the sum of the forces acting on a particle. The forces acting on a body are a combination of both surface and body forces. When this law is applied for Newtonian fluid (viscous stress is proportional to the rates of deformation), resulting equations are called as Navier-Stokes equations. The equations written below explain the momentum conservation principle (Versteeg and Malalasekera 2007):

$$\rho \frac{\partial \mathbf{v}}{\partial t} + \rho(\mathbf{v} \cdot \mathbf{grad}) \cdot \mathbf{v} = \rho \mathbf{F} - \mathbf{grad} p + \mu \Delta \mathbf{v} \tag{2}$$

Where $\mathbf{v}$ is the velocity vector with components $\mathbf{v}_x$, $\mathbf{v}_y$, $\mathbf{v}_z$ in the Cartesian system (O,x,y,z) and the vector $\mathbf{F}(Fx,F_y,F_z)$ represents the momentum source term. ρ is the density, μ is the dynamic viscosity and p represents the pressure. Since the problem at hand does not involve the heat transfer, energy equation is not considered.

2.2 About the structure

In structural mechanics problems, in general, the task is to determine deformations of solid bodies, which arise because of the action of various kinds of forces. From this, for instance, stresses in the body can be determined, which are of great importance for many applications. For the different material properties there exist a large number of material laws, which together with the balance equations lead to diversified complex equation systems for the determination of deformations (or displacements).

The basic governing equation of motion is given as (Chopra 2001):

$$m\ddot{\mathbf{u}} + c\dot{\mathbf{u}} + k\mathbf{u} = f(t) \tag{3}$$

Where m is a structural mass matrix, $\ddot{\mathbf{u}}$ is an acceleration vector, c is a structural damping matrix, $\dot{\mathbf{u}}$ is a velocity vector, k is a structural stiffness matrix, $\mathbf{u}$ is a displacement vector, f is a force vector which is a function of time, the structural damping is not involved in the finite element model so the above governing equation is modified into following form

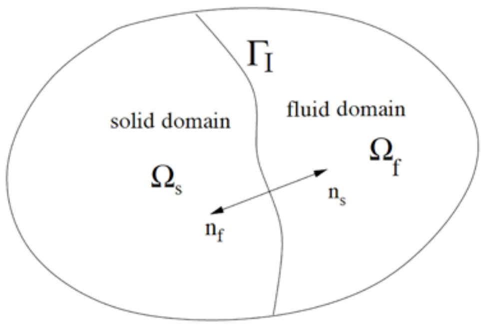

Fig. 1 Fluid-structure interface

$$m\ddot{\mathbf{u}} + k\mathbf{u} = f(t) \tag{4}$$

It is normal practice to use a numerical technique called finite element method (FEM) to find the solution for the equation Eq. (4). The basic principle behind this method of finding an approximate solution to the differential equations is to divide the volume of a structure or system into smaller (finite) elements such that infinite number of degrees of freedom (DOF) is converted to a finite value (El Maani *et al*. 2015, El Hami and Radi 1996).

2.3 Interface conditions

The main conditions at the interface (Γ_I) are the dynamic and kinematic coupling conditions. The force equilibrium requires the stress vectors to be equal as

$$\sigma^f \cdot n = \sigma^s \cdot n \quad \forall x \in \Gamma_I \tag{5}$$

also the normal velocities at interface the interface have to match as

$$\mathbf{v} \cdot n = \frac{\partial \mathbf{u}}{\partial t} \cdot n \quad \forall x \in \Gamma_I \tag{6}$$

3. Numerical discretization

The numerical computation is developed in two steps. In the first one, the conservation equations are formulated and an approach is adopted to evaluate all the terms. In the second one, a segregated, sequential solution algorithm is used to form the element matrices, to assemble them and to solve the resulting system for each variable separately ϕ (ANSYS 2013). In order to solve the governing equations of the fluid motion Eq. (2), their discretized form must first be generated. Thus, the first step is the generation of a grid, which consists of dividing the solution domain into a finite number of control volumes or computational elements.

In the second step, each term of the partial differential equation describing the flow is written in such a manner that the computer can be programmed to calculate it (Ashgriz and Mostaghimi 2002).

3.1 Finite volume discretization

The finite volume method is one of the numerical techniques applied in well established commercial CFD

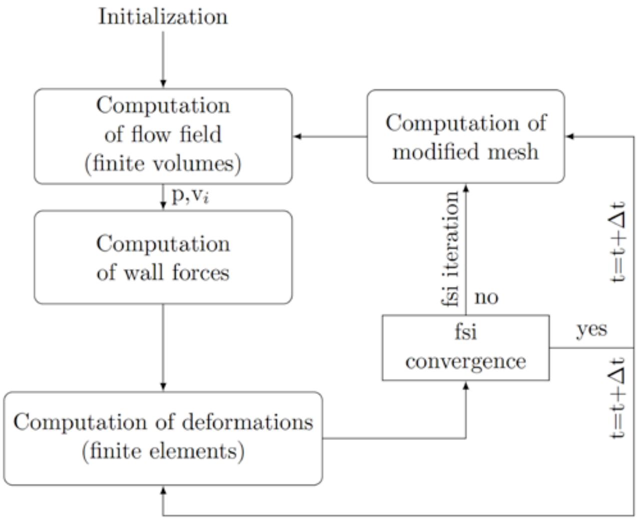

Fig. 2 Coupled solution procedure

codes to solve the governing equations of the fluid. The basic and foremost step of CFD is dividing the computational domain (geometry of the region of interest) into a large number of smaller regions called control volumes or cells and the collection of these cells is called a grid or a mesh, also, the calculated scalar values are stored at the center of the control volumes. Fluent uses the finite volume technique to convert the general transport equation into a system of algebraic equations and it uses different iterative methods to solve the algebraic equations. The following are the key steps in order to find the solution for the transport equation of a physical quantity.

The general form of transport equation in conservative form can be written as (Versteeg and Malalasekera 2007):

$$\frac{\partial(\rho\phi)}{\partial t} + div(\rho\phi\mathbf{v}) = div(\Gamma\nabla\phi) + F_\phi \tag{7}$$

where the variable ϕ can be replaced by any scalar quantity, Γ is the diffusion tensor. The left hand side of the equation contains the rate of change term and convective term, whereas the diffusive term and source term lie on the right hand side of the equation. Integrating over the control volume and applying the Gauss's divergence theorem on the general transport equation gives (Versteeg and Malalasekera 2007):

$$\frac{\partial}{\partial t}\int_{CV}\rho\phi dV + \int_A n(\rho\phi\mathbf{v})dA = \int_A n(\Gamma\nabla\phi)dA + \int_{CV} F_\phi dV \tag{8}$$

The above transport equation is subjected to the stated key steps of the finite volume technique and the discretized equation for each control volume is obtained through suitable discretization schemes. There are many spatial discretization schemes for formulating diffusive and convective terms of the transport equation (ANSYS 2013).

4. Fluid-structure treatment

4.1 Partitioned analysis

In general, one can choose to describe the whole coupled system in a monolithic way and solve all fields together or separate the fields and couple them in the sense of a partitioned analysis (Souli and Benson 2010). In the latter case either sequential (staggered) or iterative algorithms can be used. The monolithic approach is straightforward and allows solving the resulting system of equations with a complete tangent stiffness matrix (if -in an arbitrary lagrangian-eulerian (ALE) setting- fluid, structure and mesh degrees of freedom are included (Souli and Benson 2010, Huang *et al.* 2013)).

However, such monolithic approaches have a number of obvious severe drawbacks like loss of software modularity and limitations with respect to the application of different sophisticated solvers in the different fields. Hence they are generally considered not very well suited for application to real world problems, where often not only specific solution approaches but also specific codes should be used in the single fields. For this and a number of additional reasons we prefer to use a partitioned approach. The trade-off is an incomplete tangent stiffness for the overall problem. The consequences are discussed in the following section.

For the fluid-structure coupling an implicit partitioned approach is employed (Souli and Benson 2010). In Fig. 2, a schematic view of the iteration process, which is performed for each time step, is given. After the initialization, the flow field is determined in the actual flow geometry. From this, the friction and pressure forces on the interacting walls are computed, which are passed to the structural solver as boundary conditions. The structural solver computes the deformations, with which then the fluid mesh is modified, before the flow solver is started again.

The FSI iteration loop is repeated until a convergence criterion ε is reached, which is defined by the change of the mean displacements:

$$R^{FSI} = \frac{1}{N}\sum_{k=1}^{N}\frac{\left\|u_s^{k,m-1} - u_s^{k,m}\right\|_\infty}{\left\|u_s^{k,m}\right\|_\infty} \le \varepsilon \tag{9}$$

where m is the FSI iteration counter, N is the number of

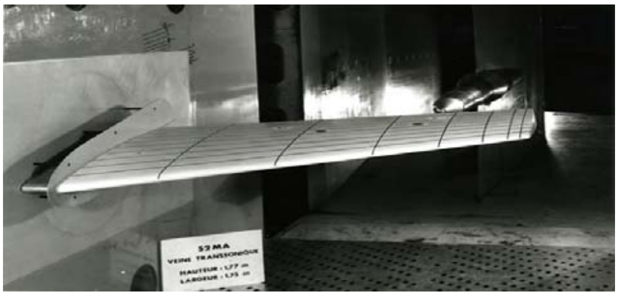

Fig. 3 M6 Wing in the ONERA S2MA wind tunnel

SWEPT WING M6

Aspect ratio A = 3.8
Taper ratio λ = 0.56
Sweep angle $\Lambda_{25\%}$ = 26.7°

ROWS OF PRESSURE TAPS

N°	y/b	upper	under
1	0.20	23	11
2	0.44	23	11
3	0.65	23	11
4	0.80	23	11
5	0.90	31	14
6	0.95	31	14
7	0.99	31	14

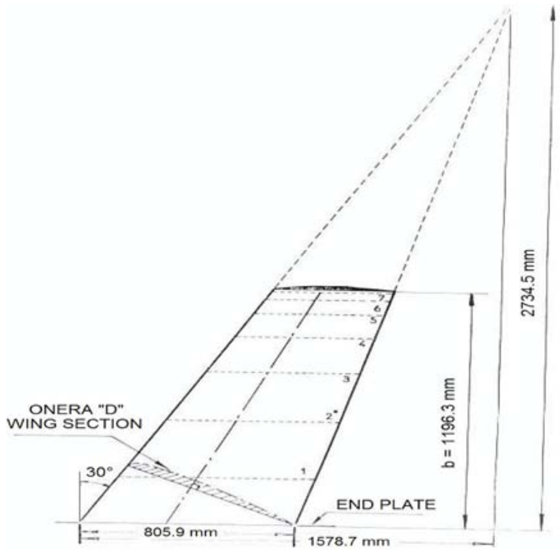

Fig. 4 Geometric layout of the ONERA M6 wing (Schmitt and Charpin 1979)

interface nodes, and $\|\cdot\|_\infty$ denotes the infinite norm (Souli and Benson 2010).

5. Validation test

5.1 Onera M6 Wing

The M6 arrow shaped Wing was designed by Bernard Monnerie and her colleagues at Onera in 1972, within the framework of cooperation within the AGARD, to serve as experimental support in studies of three-dimensional flows at transonic speeds and high Reynolds numbers and for the validation of CFD Flow Solvers (conditions representative of the actual flight of military and civilian aircraft). It has a semi-span of 1.196 m, leading edge sweep of 30° Aspect Ratio of 3.8 and Taper Ratio of 0.562, it uses a symmetric airfoil section (Schmitt and Charpin 1979). Due to the complexities of transonic flow such as shocks, local supersonic flow, and turbulent boundary layers separation, it becomes the most suitable test case for the validation of CFD solvers. The Wing Onera M6 planform is shown in the Fig. 4.

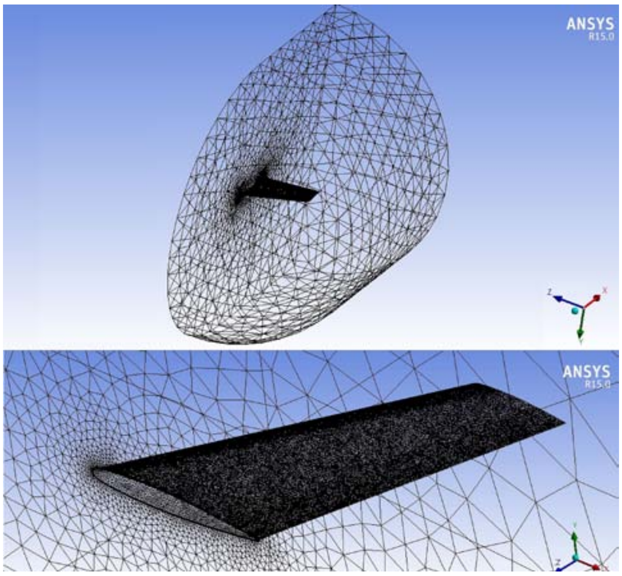

Fig. 5 Fluid mesh

Volker Schmitt and François Charpin, scientists at ONERA, recorded the results of these tests in 1979 in an AGARD report. The ONERA-M6 wing result database has been used hundreds of times to validate CFD software and is still used around the world. This is one of the most "popular" test cases, particularly suited for understanding and evaluating laminar-turbulent transition models, shock wave-boundary layer interaction models, takeoff models, etc., which are characteristic phenomena of what occurs on the wings when approaching the speed of sound.

Hybrid-unstructured mesh was generated with 375263 cells and 102432 volume nodes points for CFD computations as shown in Fig. 5. It also contains mixtures of tetrahedral, pyramids and prism cells in the boundary layer region.

The structure dynamics finite element mesh of Onera M6 wing has a total number of 20162 volume node points and 9602 surface node points. The element type for Computational Solid Dynamics (CSD) mesh is SOLID186 (twenty-node brick element with reduced integration), only used for hexahedral elements. CSD mesh is comparatively coarser than the CFD volume mesh.

5.2 Aerodynamic analysis of Onera M6 Wing

Steady aerodynamic analysis was carried out at Mach Number (M) 0.8395 at an angle of attack (α) 3.06° and Reynolds Number (Re) 11.72E6. Both one equation Spalart-Allmaras (SA) and two equations Menter Shear Stress Transport (MSST) $k-\omega$ turbulence models were

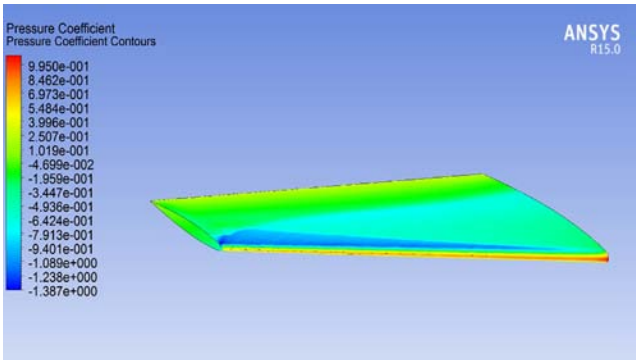

Fig. 6 Pressure distribution over the wing

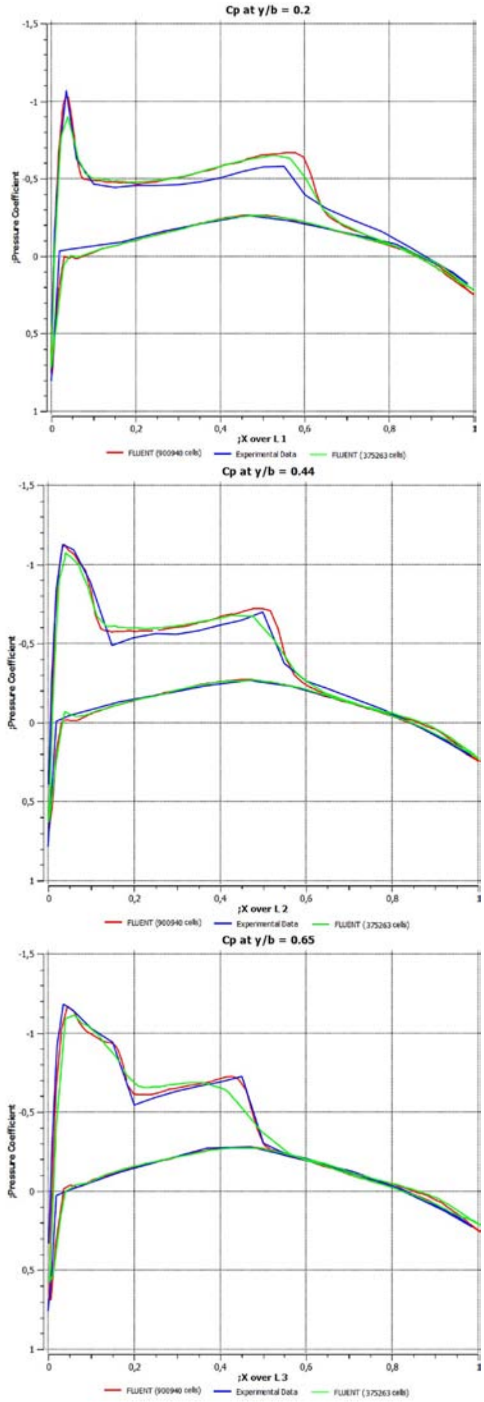

Fig. 7 C_p at *y/b*

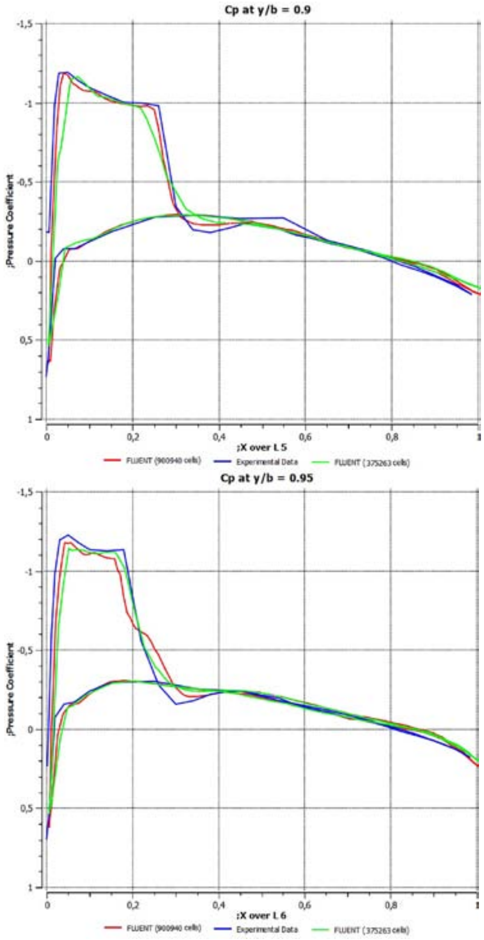

Fig. 7 Continued

used for the analysis. These steady aerodynamic calculations are performed to ensure the reliability and accuracy of the in-house code for further carrying out coupled CFD/CSD simulations.

The Pressure distribution on the wing upper surface is shown in figure Fig. 6. Strong shock has been observed on the leading edge near the root and this shock gets weaken near the wing tip whereas a strong mid chord shock has also been observed near the wing tip, resulting in to form a lambda shock. We validate our simulation results by comparing FLUENT computed data with experimental data for the Onera M6 wing.

We plot the pressure coefficient C_p at different spanwise locations of the wing and compare the results between the present simulated ones and experimental data. Here we have plotted the pressure coefficient for the spanwise locations *y/b*=0.2, 0.44, 0.65, 0.9 and 0.95.

The resultant C_p values are plotted with experimental data for comparison in Fig. 7. Experiments were conducted on M6 wing at transonic flow conditions by (Schmitt and Charpin 1979). It can be seen that generally the shock capturing is good and the location of the shock wave is correctly predicted. In spanwise location *y/b*=0.2, the shock wave is relatively less sharp and its location and resolution is not as well predicted as at other location; but as the shock wave becomes steeper along subsequent cross sections, its location and resolution improves. Overall comparison with

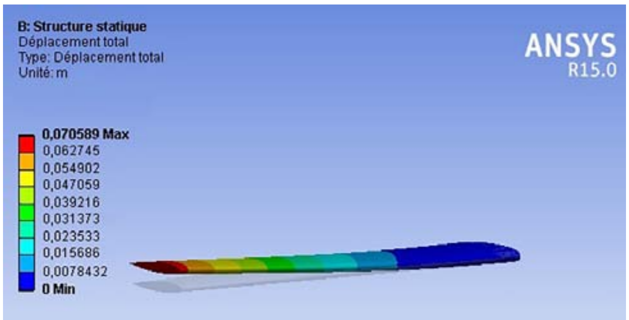

Fig. 8 Total displacement of the wing

the experimental data is good. We see that if we continue plotting the pressure coefficient spanwise, the results become less accurate due to the 3 dimensional effects far from the symmetry plane. In our plots, we have the first coarse mesh and results from our more refined mesh compared with experimental results and good agreement has been observed (Schmitt and Charpin 1979).

5.3 Aeroelastic analysis of Onera M6 Wing

In this section we consider the deformation due to aerodynamic loading of the wing by performing a steady-state one-way FSI analysis (Benra *et al.* 2011). After developing the aerodynamics loading on the wing using ANSYS/Fluent, the pressures on the wetted areas of the blade are passed as pressure loads to ANSYS/Mechanical to determine stresses and deformation on the wing. The structural configuration considered consists of an aluminum alloy which material properties are; Young's Modulus (E) is 71 GPa, Poisson's Ratio (υ) is 0.32 and material density is 2770 kg/m^3.

The computed displacement of the wing with the deformed and undeformed wing is shown in Fig. 8. It can be clearly seen that the computed fluid pressure have been successfully transferred to deform the CSD volume mesh.

5.4 Prestressed modal analysis

The eigenvalue and eigenvector problem needs to be solved for mode-frequency analyses (Jeong *et al.* 2015). It has the form of:

$$[K]\phi_i = \lambda_i [M]\phi_i \tag{10}$$

where $[K]$ is structure stiffness matrix, ϕ_i is eigenvector, λ_i is eigenvalue and $[M]$ is the structure mass matrix. For prestressed modal analyses, the $[K]$ matrix includes the stress stiffness matrix. The results of modal analysis are shown in Fig. 9. The result includes the first four mode shapes with its respective natural frequency values.

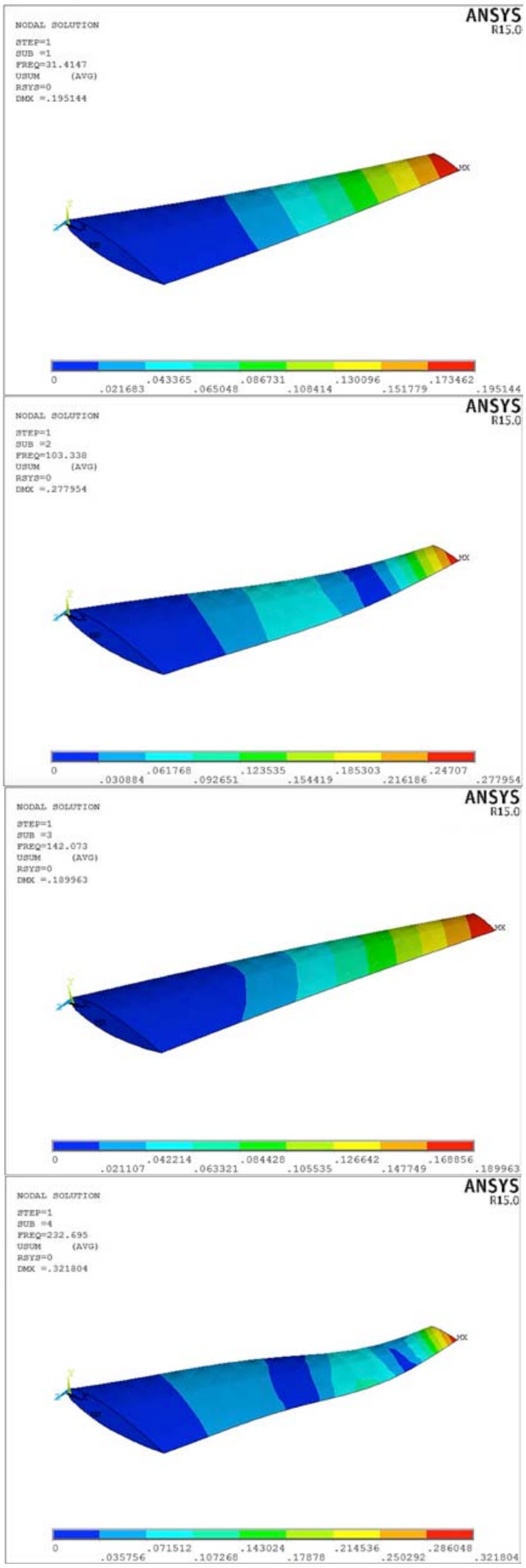

Fig. 9 The four mode shapes of the wing

6. Reliability based design optimization

The objective of the RBDO model is to design structures that should be both economic and reliable where the solution reduces the structural weight in uncritical regions. It does not only provide an improved design but also a higher level of confidence in the design. The classical approach (El Hami and Radi 2013) can be carried out in two separate spaces: the physical space and the normalized space. Since very many repeated searches are needed in the above two spaces, the computational time for such an optimization is a big problem. To overcome these difficulties, two points of view have been considered. From reliability viewpoint, RBDO involves the evaluation of probabilistic constraints, which can be executed in two different ways: either using the Reliability Index Approach (RIA), or the Performance Measure Approach (PMA) (Tu *et al.* 1999, Youn *et al.* 2003). However, from optimization viewpoint, Kharmanda *et al.* (2004) have elaborated an efficient method called the Hybrid Method (HM) where the optimization process is carried out in a Hybrid Design Space (HDS). This method has been shown to verify the optimality conditions relative to the classical RBDO method. The advantage of the hybrid method allows us to satisfy a required reliability level for different cases (static, dynamic…), but the vector of variables here contains both deterministic and random variables. The hybrid RBDO problem is thus more complex than that of deterministic design (Beyaoui *et al.* 2016, Dalton *et al.* 2013). The major difficulty lies in the evaluation of the structural reliability, which is carried out by a special optimization procedure. For a special case, when a failure interval $[f_a, f_b]$ is given, HM can be used with a big implementation complexity and high computing time. So there is a strong motivation to develop a new technique that can overcome both drawbacks.

Using the Deterministic Design Optimization (DDO) procedure by a reliability analysis (see Kharmanda *et al.* (2004)), we can distinguish between two cases:

Case 1: High reliability level: when choosing high values of safety factors for certain parameters, the structural cost (or weight) will be significantly increased because the reliability level becomes much higher than the required level for the structure. So, the design is safe but very expensive.

Case 2: Low reliability level: when choosing small values of safety factors or bad distribution of these factors, the structural reliability level may be too low to be appropriate. For example, (Grandhi and Wang 1998) found that the resulting reliability index of the optimum deterministic design of a gas turbine blade is under some uncertainties. This result indicated that the reliability at the deterministic optimum is quite low and needs to be improved by probabilistic design.

For both cases, we can find that there is a strong need to integrate the reliability analysis in the optimization process in order to control the reliability level and to minimize the structural cost or weight in the non-critical regions of the structure (El Hami and Radi 2013, Al Kheer *et al.* 2011).

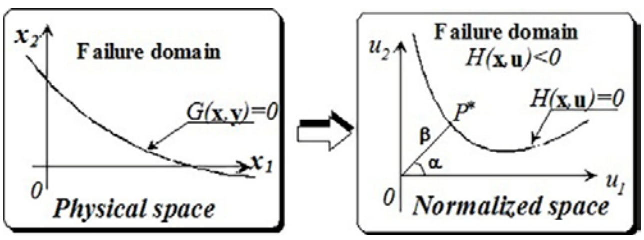

Fig. 10 Transformation between the physical space and normalized one

6.1 Classical Method (CM)

Traditionally, for the reliability-based optimization procedure we use two spaces: the physical space and the normalized space (Fig. 10). Therefore, nesting the two following problems performs the reliability-based optimization:

6.1.1 Optimization problem

$$\begin{cases} \min: \quad f(\mathbf{x}) \\ \text{subject to:} \quad g_k(\mathbf{x}) \le 0 \\ \qquad\qquad \beta(\mathbf{x},\mathbf{u}) \ge \beta_t \end{cases} \tag{11}$$

where $f(\mathbf{x})$ is the objective function, $g_k(\mathbf{x})\le 0$ and $\beta(\mathbf{x},\mathbf{u})\ge\beta_t$ are the associated constraints, $\beta(\mathbf{x},\mathbf{u})$ is the reliability index of the structure and β_t is the target reliability.

6.1.2 Reliability analysis

The reliability index $\beta(\mathbf{x},\mathbf{u})$ is determined by solving the minimization problem (El Hami and Radi 2013)

$$\begin{cases} \beta = \min \operatorname{dis}(\mathbf{u}) = \sqrt{\sum_1^m u_j^2} \\ \text{subject to:} \quad H(\mathbf{x},\mathbf{u}) \le 0 \end{cases} \tag{12}$$

where dis($\mathbf{u}$) is the distance in the normalized random space and $H(\mathbf{x},\mathbf{u})$ is the performance function (or limit state function) in the normalized space, defined such that $H(\mathbf{x},\mathbf{u})\le 0$ implies failure.

In the physical space, the image of $H(\mathbf{x},\mathbf{u})$ is the limit state function $G(\mathbf{x},\mathbf{y})$, see Fig. 10. The solution of these nested problems leads to very large computational time, especially for large-scale structures (Radi and El Hami 2007, Moro *et al.* 2002).

6.2 Hybrid Method (HM)

In order to improve the numerical performance, the hybrid approach consists in minimizing a new form of the objective function $F(\mathbf{x},\mathbf{y})$ subject to a limit state and to deterministic as well as to reliability constraints, as

$$\begin{cases} \min\limits_{\mathbf{x},\mathbf{y}}: \quad F(\mathbf{x},\mathbf{y}) = f(\mathbf{x}).\, d_\beta(\mathbf{x},\mathbf{y}) \\ \text{subject to:} \quad G(\mathbf{x},\mathbf{y}) \le 0 \\ \qquad\qquad g_k(\mathbf{x}) \le 0 \\ \qquad\qquad d_\beta(\mathbf{x},\mathbf{y}) \ge \beta_t \end{cases} \tag{13}$$

Here, $d_\beta(\mathbf{x},\mathbf{y})$ is the distance in the hybrid space between the optimum and the design point, $d_\beta(\mathbf{x},\mathbf{y})$=dis($\mathbf{u}$).

The minimization of the function $F(\mathbf{x},\mathbf{y})$ is carried out in the Hybrid Design Space (HDS) of deterministic variables $\mathbf{x}$ and random variables $\mathbf{y}$. We can see two important points: the optimal solution and the reliability solution. In fact, when using the HM, we have a complex optimization problem with many variables. Solving this problem, we get a local optimum. When changing the starting point, we may get another local optimum. This way the designer has to repeat the optimization process to get several local optima (Kharmanda *et al.* 2004).

7. Proposed Safest Point method (SP)

In the modal studies (Fig. 9), in order to avoid the failure domain, we consider a frequency interval [f_a, f_b]. Here, the frequency of the vibrating structure should not work in this interval. When an explicit description displacement/frequency is supplied to the designer, it is easy to define an analytically suitable interval [f_a, f_b] that corresponds to the safest structure. However, when we have an implicit model, we need an optimization procedure to determine the safest area. We have two ways to provide the required frequency constraints:

- The first way is to supply the designer with an eigen-frequency value as a constraint to be respected. Here, we consider a safest interval as a probabilistic constraint. Then, the hybrid method can be used with some implementations but leads to many complexities and computing time problems (Mohsine and El Hami 2010).
- The second way is to supply the designer with a failure interval [f_a, f_b] as a constraint and the eigen-frequency f_n corresponding to the safest position in this interval needs a probabilistic equality constraint (β_a=β_b); here the HM can be used but it has a big implementation complexity and high computing time consumption (El Hami and Radi 2011).

So there is a strong motivation to develop a new technique that can overcome these drawbacks. In this section, we develop a new method, called Safest Point (SP) method. We consider a given interval [f_a, f_b] (generally given by the technical specifications) for the first shape mode, where the safest point has the same reliability index relative to both sides of the interval (see Fig. 11).

We consider the equality of the reliability indices

$$\beta_a = \beta_b \tag{14}$$

with $\beta_a = \sqrt{\sum_{i=1}^{n} \left(u_i^a\right)^2}$ and $\beta_b = \sqrt{\sum_{i=1}^{n} \left(u_i^b\right)^2}$ $\quad i = 1,\ldots,n$

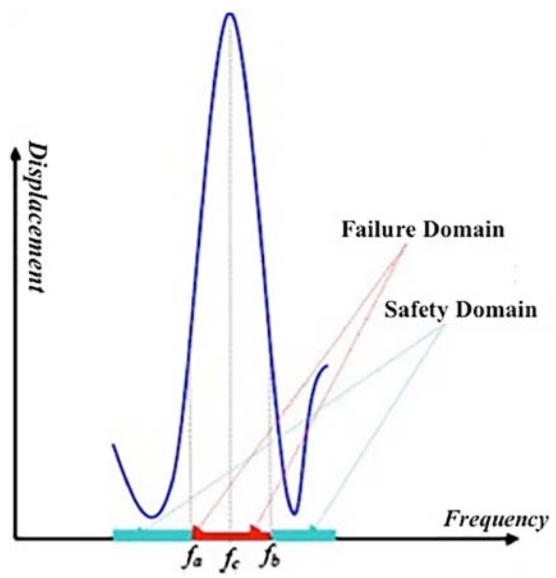

Fig. 11 The safest point at frequency f_n

The equality (14) gives the equality of each term. So we have

$$u_i^a = -u_i^b \qquad \text{i=1,…,n} \tag{15}$$

We write the SP method for two distribution laws:

• *Normal distribution for SP method*

One of the most commonly used distributions of a random variable y_i in engineering problems is the normal or Gaussian distribution. The mean value m_i and the standard deviation σ_i are two parameters of the distribution, usually estimated from available data. The normalized variable u_i is defined by

$$u_i = \frac{y_i - m_i}{\sigma_i} \qquad i = 1,\ldots,n \tag{16}$$

According to the Eq. (16), we get

$$\frac{y_i^a - m_i}{\sigma_i} = -\frac{y_i^b - m_i}{\sigma_i} \qquad \text{i=1,...,n} \tag{17}$$

or: $\dfrac{y_i^a - x_i}{\sigma_i} = -\dfrac{y_i^b - x_i}{\sigma_i}$

To obtain equality between the reliability indices (see Eq. (14)), the mean value of variable corresponds to the structure at f_n. So the mean values of safest solution are located in the middle of the variable interval $[y_i^a, y_i^b]$ as follows

$$m_i = x_i = \frac{y_i^a + y_i^b}{2} \qquad i = 1,\ldots,n \tag{18}$$

• *Log-normal distribution for SP method*

The normalized variable u_i is this case is defined as

$$u_i = \frac{ln(y_i) - \mu_i}{\xi_i} \qquad i = 1,\ldots,n \tag{19}$$

where μ_i and ξ_i are the distribution parameters of the log-normal law, given by

$$\mu_i = \ln\left(\frac{x_i}{\sqrt{1+\gamma_i^2}}\right), \quad \xi_i = \sqrt{\ln\left(1+\gamma_i^2\right)} \qquad i = 1,\ldots,n \tag{20}$$

and $\gamma_i = \dfrac{\sigma_i}{x_i} \qquad i = 1,\ldots,n.$.

The normalized variable u_i is then expressed by

$$u_i = \frac{\ln\left(\dfrac{y_i\sqrt{1+(\sigma_i/x_i)^2}}{x_i}\right)}{\sqrt{\ln(1+(\sigma_i/x_i)^2)}}, \qquad i = 1,\ldots,n \tag{21}$$

According to Eq. (16), we get

$$\frac{\ln\left(y_i^a\right) - \mu_i}{\xi_i} = -\frac{\ln\left(y_i^b\right) - \mu_i}{\xi_i} \qquad i = 1,\ldots,n \tag{22}$$

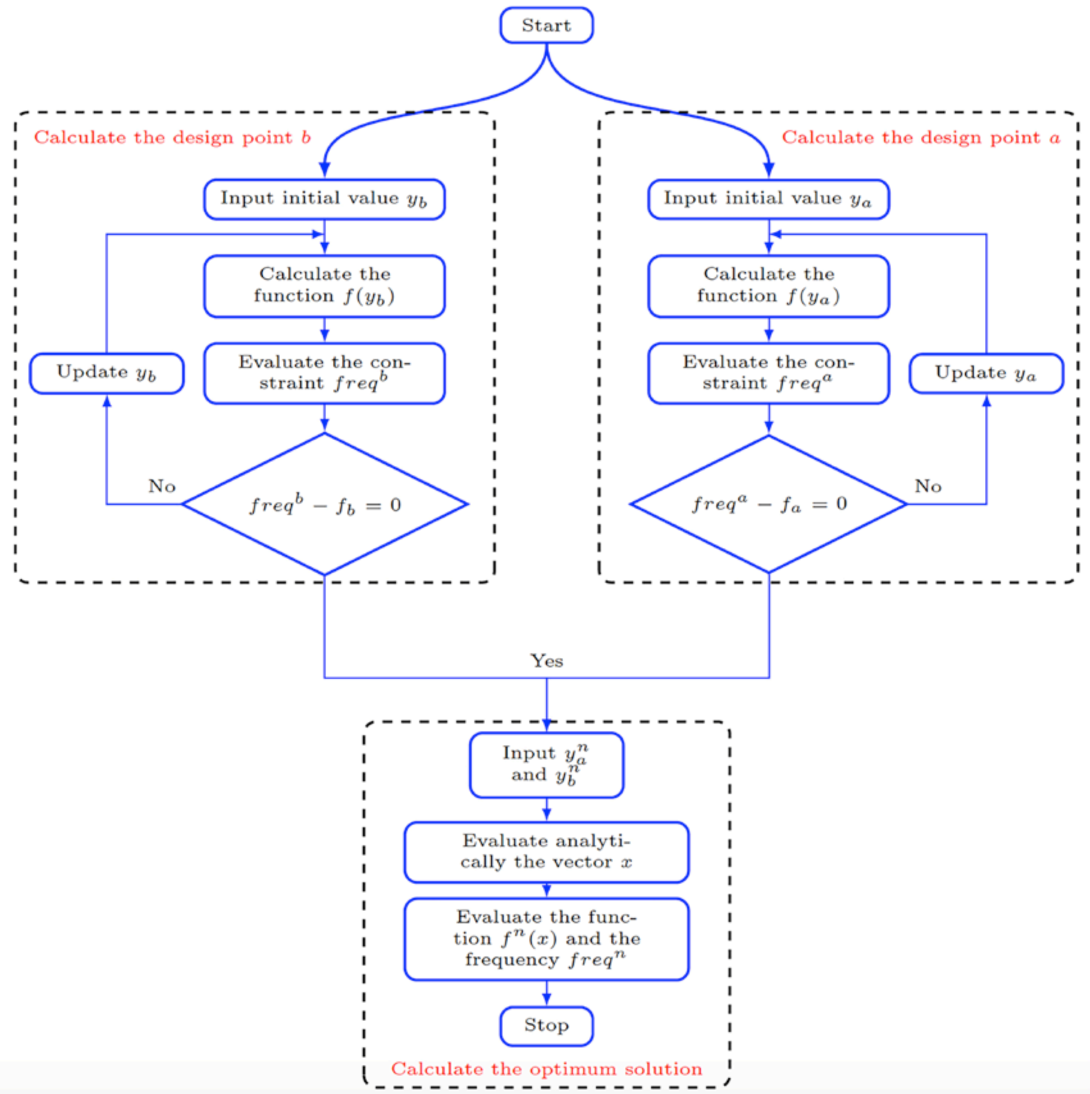

Fig. 12 SP method

So the safest point corresponding to the frequency f_n and located in the interval $[f_a, f_b]$ is given by

$$m_i = x_i = \sqrt{1+\gamma_i^2}\exp\left(\frac{\ln(y_i^a \cdot y_i^b)}{2}\right) \qquad i = 1,\ldots,n \quad (23)$$

Generally, one can find the SP method using normal distribution. In this paper we propose the SP method using also log-normal distribution which is very adequate for the non-linear problems. Other distributions can be used such as uniform law.

7.1 Implementation of the SP approach

The SP algorithm for symmetric case can be expressed by the three following steps (two sequential optimization steps and an analytical evaluation one) (see Fig. 12):

1. Compute the design point a: The first optimization problem is to minimize the objective function subject to the first bound of the frequency interval f_a. The resulting solution is considered as a most probable point A.
2. Compute the design point b: The second optimization problem is to minimize the objective function subject to the second bound of the frequency interval f_b. The resulting solution is considered as a most probable point B.
3. Compute the optimum solution: Here, we analytically determine the optimum solution of the studied structure using Eqs. (18)-(23) for linear and non-linear distributions cases.

The reliability-based optimum structure under free vibrations for a given interval of eign-frequency is found at the safest position of this interval where the safest point has the same reliability index relative to both sides of the interval. A simple method has been proposed here to meet the safest point requirements relative to a given frequency interval.

8. Numerical simulation of RBDO on Aircraft Wing

The chord of the Airfoil has dimensions and orientation as shown in Fig. 13 and Table 1:

Table 1 Parameterization of the Airfoil

Variables	A_N	B_N	C_N	D_N
Dimensions (m)	0.054	0.092	0.096	0.044

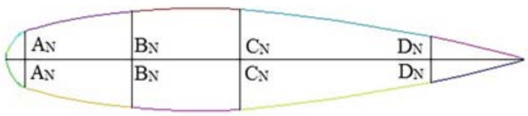

Fig. 13 Dimensions of the Airfoil

Table 2 Results for the SP method

Variables	Parameters	Initial	Normal distribution	Log-normal distribution
F_N	A_N (m)	0.054	0.040826	0.038582
	B_N (m)	0.092	0.069145	0.070540
	C_N (m)	0.096	0.095406	0.095833
	D_N (m)	0.044	0.037493	0.035276
F_A	A_1 (m)	0.027	0.027285	0.027285
	B_1 (m)	0.046	0.046169	0.046169
	C_1 (m)	0.048	0.082863	0.082863
	D_1 (m)	0.022	0.028582	0.028582
F_B	A_2 (m)	0.081	0.054367	0.054367
	B_2 (m)	0.138	0.092121	0.092121
	C_2 (m)	0.144	0.10795	0.10795
	D_2 (m)	0.066	0.046404	0.046404
State variables	F_A (Hz)	23.746	24.998	24.998
	F_B (Hz)	46.788	34.003	34.003
	F_N (Hz)	31.414	29.102	29.102
	Mass (Kg)	411.310	359.855	356.410
	Time (s)	-	1100	1100

The main objective is to minimize the volume of the wing subject to the constraint of the first eigen-frequency for a given interval [25, 35], that is located on the safest position of this interval; the system must also meet predetermined target reliability. So $F_a = 25$ Hz , $F_b = 35$ Hz, and $F_n = ?$ Hz, where F_n must verify the equality of reliability indices: $\beta_a = \beta_b$.

The choice of the target index is usually done by statistical studies but here we consider the index of reliability target as $\beta_t = 3$ which indicates a very small probability of failure.

We have two simple optimization problems:

- The first is to minimize the objective function of the first model subject to the frequency f_a constraint as follows

$$\begin{cases} \min\limits_{A_1,\dots} : \; Vol_a(A_1, B_1, C_1, D_1) \\ \text{subject to} : f_{\max}^1(A_1, B_1, C_1, D_1) - f_a = 0 \end{cases} \tag{24}$$

- The second is to minimize the objective function of the second model subject to the frequency f_b constraint as follows

$$\begin{cases} \min\limits_{A_2,\dots} : \; Vol_b(A_2, B_2, C_2, D_2) \\ \text{subject to} : f_{\max}^2(A_2, B_2, C_2, D_2) - f_b = 0 \end{cases} \tag{25}$$

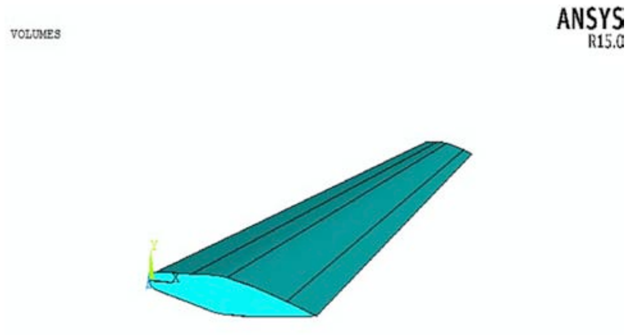

Fig. 14 Optimized form of the aircraft wing

and next we compute the coordinates of the third model which corresponds to f_n according to Eq. (18). Table 2 shows the results of the SP method and presents the reliability-based optimum point for a given interval [25,35].

The resulting design obtained by the SP method gives the minimum volume where the objective is to provide the best compromise between cost and safety. The SP methodology satisfies the required reliability level β=3 (which indicates a very small probability of failure) and gives a smaller structural volume than the first volume for the reliability level. The SP method reduces the high computing time due to its analytical evaluation of the computing results comparing to the large number of iterations of the classical and hybrid method. It can be considered as semi-numerical method and it is simple to be implemented on the machine.

This method defines the eigen-frequency of a given interval and provides the designer with reliability-based optimum solution with a small tolerance in fluid-structure interaction problems.

9. Conclusions

The objective of this work was to quantify the influence of material and operational uncertainties on the performance of the interaction that occurs between a structure and a fluid flow based on generated aerodynamic loads, considered as a non-linear and complex system, and to give a description of the most common advantages of the proposed RBDO method in a way to reduce the structural weight in uncritical regions of the design process. It provides an improved design and a higher level of confidence in the design. The classical RBDO approach can be carried out in two separate spaces: the physical space and the normalized space. Since very many repeated searches are needed in the above two spaces, the computational time for each optimization step is a big problem. For this reasons the structural engineers do not consider the RBDO as a practical tool for design optimization. Based on the reduction of the computing time, we proposed here a new methodology called Safest Point method (SP) used for linear distributions and extended here for non-linear distributions in order to solve the freely vibrating structures in the context of the fluid-structure interaction problems.

Acknowledgements

The authors would like to thank “Erasmus Mundus Programme, Action 2-STRAND 1, Lot 1, North AfricaCountries” for their financial support for the realization of this work.

References

Abbasnia, R., Shayanfar, M. and Khodam, A. (2014), “Reliability-based design optimization of structural systems using a hybrid genetic algorithm”, *Struct. Eng. Mech.*, **52**(6), 1099-1120.

Al Kheer, A.A., El Hami, A. and Kharmanda, M.G. (2011), “Reliability based design for soil tillage machines”, *J. Terramech.*, **48**(1), 57-64.

ANSYS Inc. (2013), Ansys Fluent Theory.

Ashgriz, N. and Mostaghimi, J. (2002), *Fluid Flow Handbook*, McGraw-Hill Handbooks, Ch. An Introduction to Computational Fluid Dynamics.

Benra, F., Dohmen, H., Pei, J., Schuster, S. and Wan, B. (2011), “A comparison of one-way and two-way coupling methods for numerical analysis of fluid structure interactions”, *J. Appl. Math.*, **2011**, 40-56.

Beyaoui, M., Guerine, A., Walha, L., El Hami, A., Fakhfakh, T. and Haddar, M. (2016), “Dynamic behavior of the one-stage gear system with uncertainties”, *Struct. Eng. Mech.*, **58**(3), 443-458.

Chopra, A. (2001), *Dynamics of Structures*, 2nd Edition, Pearson Prentice Hall.

Dalton, S. K., Atamturktur, S., Farajpour, I. and Juang, C. H. (2013), “An optimization based approach for structural design considering safety, robustness and cost”, *Eng. Struct.*, **57**, 356-363.

El Hami, A. and Radi, B. (1996), “Some decomposition methods in the analysis of repetitive structures”, *Comput. Struct.*, **58**(5), 973-980.

El Hami, A. and Radi, B. (2011), “Comparison study of different reliability-based design optimization approaches”, *Adv. Mater. Res.*, **274**, 119-130.

El Hami, A. and Radi, B. (2013), *Incertitudes, Optimisation et Fiabilité des Structures*, Hermès, Paris.

El Hami, A. and Radi, B. (2013), *Uncertainty and Optimization in Structural Mechanics*, Wiley.

El Maani, R., Radi, B. and El Hami, A. (2015), “Reliability study of a coupled three dimensional system with uncertain parameters”, *J. Adv. Mater. Res.*, **1099**, 87-93.

Grandhi, R. and Wang, L. (1998), “Reliability-based structural optimization using improved two-point adaptive nonlinear approximations”, *Finite Elem. Anal. Des.*, **29**, 35-48.

Huang, S., Li, R. and Li, Q.S. (2013), “Numerical simulation on fluid-structure interaction of wind around super-tall building at high Reynolds number conditions”, *Struct. Eng. Mech.*, **46**(2), 197-212.

Jeong, K., Ahn, B. and Lee, S. (2001), “Modal analysis of perforated rectangular plates in contact with water”, *Struct. Eng. Mech.*, **12**(2), 189-200.

Kharmanda, G., El Hami, A. and Olhoff, N. (2004), *Frontiers on Global Optimization*, Kluwer Academic, Ch. Global Reliability Based Design Optimization, 255-274.

Mohsine, A. and El Hami, A. (2010), “A robust study of reliability-based optimization methods under eigen-frequency”, *Comput. Meth. Appl. Mech. Eng.*, **199**, 1006-1018.

Moro, T., El Hami, A. and Moudni, A.E. (2002), “Reliability analysis of a mechanical contact between deformable solids”, *A Probab. Eng. Mech.*, **17**(3), 227-232.

Radi, B. and El Hami, A. (2007), “Reliability analysis of the metal forming process”, *Math. Comput. Model.*, **45**(3-4), 431-439.

Schmitt, V. and Charpin, F. (1979), “Pressure distributions on the onera m6 wing at transonic mach numbers”, Agard-ar-138-experimental database for computer program assessment.

Souli, M. and Benson, D. J. (2010), *Arbitrary Lagrangian-Eulerian and Fluid-Structure Interaction*, ISTE Ltd and John Wiley & Sons.

Tu, J., Choi, K. and Park, Y. (1999), “A new study on reliability-based design optimization”, *J. Mech. Des.*, **121**(4), 557-564.

Versteeg, H. and Malalasekera, W. (2007), *An Introduction to Computational Fluid Dynamics*, 2nd Edition, Pearson Prentice Hall.

Youn, B., Choi, K. and Park, Y. (2003), “Hybrid analysis method for reliability-based design optimization”, *J. Mech. Des.*, **25**(2), 221-232.

Yun, Z. and Hui, Y. (2011), “Coupled fluid structure flutter analysis of a transonic fan”, *Chin. J. Aeronaut.*, **24**, 258-264.

CC